3-13-2020

Inhibiting Iron Mobilization from Bacterioferritin in Pseudomonas aeruginosa Impairs Biofilm Formation Irrespective of Environmental Iron Availability

Anabel Soldano
Louisiana State University

Huili Yao
Louisiana State University

Josephine R. Chandler
University of Kansas, Lawrence

Mario Rivera
Louisiana State University

Recommended Citation

Soldano, A., Yao, H., Chandler, J., & Rivera, M. (2020). Inhibiting Iron Mobilization from Bacterioferritin in Pseudomonas aeruginosa Impairs Biofilm Formation Irrespective of Environmental Iron Availability. *ACS Infectious Diseases, 6* (3), 447-458. https://doi.org/10.1021/acsinfecdis.9b00398

ACS Infectious Diseases

pubs.acs.org/journal/aidcbc

Article

Inhibiting Iron Mobilization from Bacterioferritin in *Pseudomonas aeruginosa* Impairs Biofilm Formation Irrespective of Environmental Iron Availability

Anabel Soldano, Huili Yao, Josephine R. Chandler, and Mario Rivera*

Cite This: *ACS Infect. Dis.* 2020, 6, 447−458

Read Online

ACCESS | Metrics & More | Article Recommendations | Supporting Information

ABSTRACT: Although iron is essential for bacteria, the nutrient presents problems of toxicity and solubility. Bacteria circumvent these problems with the aid of iron storage proteins where Fe^{3+} is deposited and, when necessary, mobilized as Fe^{2+} for metabolic requirements. In *Pseudomonas aeruginosa*, Fe^{3+} is compartmentalized in bacterioferritin (BfrB), and its mobilization as Fe^{2+} requires specific binding of a ferredoxin (Bfd) to reduce the stored Fe^{3+}. Blocking the BfrB-Bfd complex leads to irreversible iron accumulation in BfrB and cytosolic iron deprivation. Consequently, given the intracellular iron sufficiency requirement for biofilm development, we hypothesized that blocking the BfrB-Bfd interaction in *P. aeruginosa* would impair biofilm development. Our results show that planktonic and biofilm-embedded cells where the BfrB-Bfd complex is blocked exhibit cytosolic iron deficiency, and poorly developed biofilms, even in iron-sufficient culture conditions. These results underscore inhibition of the BfrB-Bfd complex as a rational target to dysregulate iron homeostasis and possibly control biofilms.

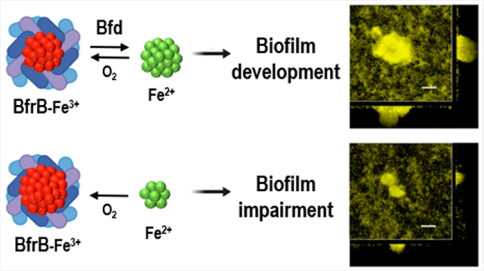

KEYWORDS: *iron homeostasis, iron metabolism, biofilm, pellicles, biofilm dispersion, Pseudomonas aeruginosa, bacterioferritin, ferredoxin, protein−protein interactions*

Biofilms are formed by sessile bacterial communities growing on surfaces or at interfaces, embedded in a self-produced matrix of biopolymers typically consisting of DNA, proteins, and polysaccharides.[1,2] Bacterial cells in biofilms often exhibit increased resistance to host-immune responses and elevated tolerance to antibiotic therapy.[3] *Pseudomonas aeruginosa* is one of the leading pathogens associated with hospital infections due to its propensity to colonize urinary catheters and endotracheal tubes.[4] The ability of *P. aeruginosa* to form biofilms on indwelling medical devices and in the lungs of cystic fibrosis patients is thought to account for the recalcitrant infections and low efficiency of existing therapies.[5,6] Complex regulatory networks influenced by a variety of environmental cues and involving a number of intra- and extracellular secondary messengers, such as quorum sensing molecules, cyclic diguanosine-5′-monophosphate (c-di-GMP), and small RNAs,[7] signal the transition from planktonic to biofilm lifestyle, or vice versa. Iron also serves as a signal in the development or dispersion of *P. aeruginosa* biofilms.[8] Iron is essential for bacteria because of its participation in multiple fundamental enzymatic reactions and important metabolic processes such as respiration. To establish an infection, pathogenic bacteria are obligated to procure iron from the host, but the host severely restricts iron availability via a process termed nutritional immunity.[9−11] In addition, the extremely low solubility of the Fe^{3+} ion at physiological pH and the reactivity of the soluble Fe^{2+} ion toward O_2 and H_2O_2 place additional burdens that demand extremely tight regulation of bacterial iron homeostasis processes (acquisition, storage, and utilization).[12,13] The significance of iron restriction/availability during infection has been underscored in a murine model of infection, where it was demonstrated that one injection of iron decreased the mean lethal dose (LD_{50}) of *P. aeruginosa* by a factor of ∼100,000.[14]

P. aeruginosa biofilms in medical settings are often associated with chronic infections, enhanced tolerance toward antibiotics, and increased resistance toward immune responses.[3,15] Consequently, strategies directed at preventing or dispersing biofilms are important. In this context, there is a clear interdependence between bacterial iron acquisition and biofilm formation.[8] The critical role played by iron in biofilm development was initially uncovered by the discovery that lactoferrin, which binds Fe^{3+} with very high affinity, prevents *P. aeruginosa* cells from forming biofilms.[16] The same study suggested that high iron levels signal *P. aeruginosa* to form microcolonies and eventually mature biofilms, whereas low iron levels discourage biofilm growth. Subsequent studies established that the development of mature biofilms requires

Received: October 18, 2019
Published: January 3, 2020

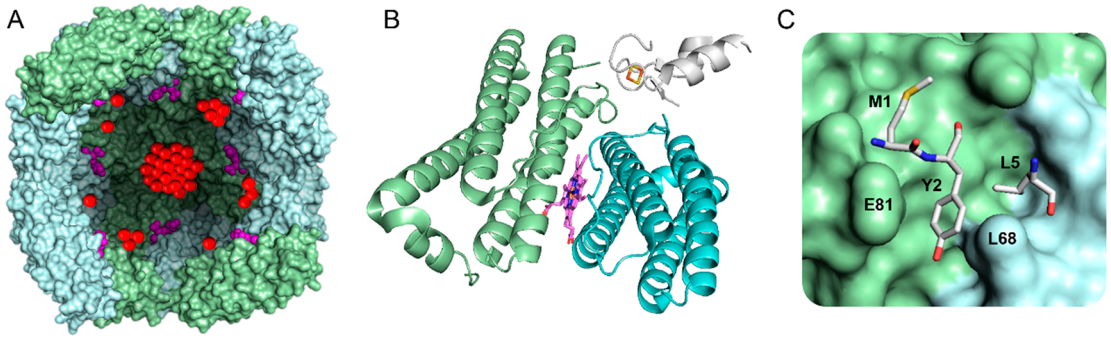

Figure 1. Mobilization of iron stored in BrfB into the *P. aeruginosa* cytosol requires a specific interaction with Bfd. (A) Fe^{3+} (red spheres) is stored in the interior cavity (~80 Å in diameter) of BfrB, a spherical, hollow protein assembled from 24 subunits (green and cyan) and heme molecules (violet spheres) (PDB ID 3is7). (B) Bfd (gray) binds BfrB at the interface of two subunits, above a heme molecule (violet sticks) (PDB ID 4e6k) to facilitate electron transfer from the [2Fe-2S] cluster in Bfd (red and yellow sticks) to the Fe^{3+} stored in BfrB via a heme molecule, to facilitate the mobilization of Fe^{2+}. (C) Closeup view of the BfrB-Bfd interface illustrating the set of interactions between L68 and E81 in BfrB (cyan and green) and M1, Y2, and L5 in Bfd (gray sticks).

sufficient environmental iron, active iron uptake mechanisms, and sufficient intracellular iron reserves.[17,18] These ideas were substantiated in additional investigations showing that iron chelators such as ethylenediaminetetraacetic acid (EDTA), diethyelenetriamine pentaacetic acid (DTPA), or deferasirox exert a negative impact on *P. aeruginosa* biofilm formation.[19,20] Gallium has also been shown to compromise iron metabolism and biofilm formation.[21,22] Ga^{3+}, which has an ionic radius similar to that of Fe^{3+}, is thought to incorporate into iron-utilizing proteins and enzymes, but since Ga^{3+} cannot be reduced in the cell, these proteins become inhibited, adversely affecting iron homeostasis and other metabolic paths. Systemic gallium treatment is being explored as a strategy that alters iron homeostasis and improves lung function in patients with chronic *P. aeruginosa* infection.[23] Taken together, these findings suggest that iron metabolism presents an important bacterial vulnerability to be addressed in the search of novel strategies to combat antibiotic resistance and biofilm infections.

Recent studies suggest that bacterial iron metabolism can be dysregulated by interfering with the process of iron storage/mobilization from bacterioferritin (BfrB), the main iron storage protein in *P. aeruginosa*.[12,24] BfrB is a roughly spherical and hollow protein with an interior cavity that can store up to ~3000 Fe^{3+} ions in the form of a mineral (Figure 1A).[25] Bacterioferritins, which exist only in bacteria, are characterized by their ability to bind heme.[26] Mobilization of Fe^{3+} stored in BfrB requires specific interactions with a ferredoxin (Bfd),[26−28] which has been shown to exhibit a fold distinct from other ferredoxins of known structure.[29] X-ray crystallography showed that Bfd binds BfrB at the interface of subunit dimers, above a heme molecule (Figure 1B), and characterization of the complex in solution showed that the dissociation constant (K_d) for the BfrB-Bfd interaction is 3 μM.[30] Detailed analysis of the BfrB-Bfd interface showed that the stability of the complex depends strongly on a continuous set of contacts between L68 and E81 in BfrB and M1, Y2, and L5 in Bfd (Figure 1C). In agreement with the crucial role of these residues on the stability of the BfrB-Bfd complex, replacing L68 or E81 in BfrB with alanine results in an approximately 100-fold increase in the magnitude of the K_d, whereas the association between Bfd and the L68A/E81A double mutant of BfrB is undetectable. The inability of Bfd to bind to the mutant bacterioferritin inhibits iron mobilization from L68A/E81A BfrB.[30] These *in vitro* observations have been recently recapitulated in *P. aeruginosa* cells, where it was demonstrated that blocking the BfrB-Bfd interaction by either deleting the *bfd* gene (Δ*bfd*), or by replacing the wild type *bfrB* gene with a L68A/E81A double mutant *bfrB* allele [*bfrB*(L68A/E81A)], results in the irreversible accumulation of iron in BfrB. The irreversible accumulation of iron in BfrB, in turn, causes iron deprivation in the *P. aeruginosa* cytosol and triggers an acute iron starvation response.[12]

Given that *P. aeruginosa* requires sufficient intracellular iron to establish mature biofilms,[17] we reasoned that the iron deficiency that ensues in the cytosol of the Δ*bfd* or *bfrB*(L68A/E81A) mutants might adversely affect biofilm formation, independently of the environmental iron levels. To probe these ideas, we studied the biofilm formation propensity of the Δ*bfd* and *bfrB*(L68A/E81A) mutants and found that, in agreement with our expectations, the mutants form thin and spotted pellicles at the air−liquid interface, which are distinct from the robust and homogeneous pellicles formed by the wild type cells. Similarly, surface-attached biofilms formed by the Δ*bfd* and *bfrB*(L68A/E81A) mutants in flow cells contain significantly less biomass than those formed by the wild type strain under identical growth conditions. These findings indicate that interfering with the BfrB-Bfd complex in *P. aeruginosa* is a viable rational strategy to combat biofilms in a manner that is independent of the environmental iron concentration, and therefore does not require the addition of chelating agents or iron binding proteins.

RESULTS AND DISCUSSION

Blocking the BfrB-Bfd Interaction in *P. aeruginosa* Impairs Pellicle Formation. *P. aeruginosa*, like most bacteria, forms different types of biofilm depending on the environmental conditions. In the laboratory, *P. aeruginosa* can grow as colony biofilms on solid agar media, as surface-associated submerged biofilms under continuous flow, or as pellicles at the air−liquid interface when cultured without agitation (statically).[31,32] To study the effect of iron homeostasis dysregulation on pellicle formation, wild type, Δ*bfd*, and *bfrB*(L68A/E81A) cells were cultured in 24-well plates at 30 °C under static conditions in iron replete (20 μM) PI media. The planktonic growth was monitored by the time-dependent enumeration of planktonic cells, while the development of pellicles was followed with the aid of microscopy and by crystal

https://dx.doi.org/10.1021/acsinfecdis.9b00398
ACS Infect. Dis. 2020, 6, 447−458

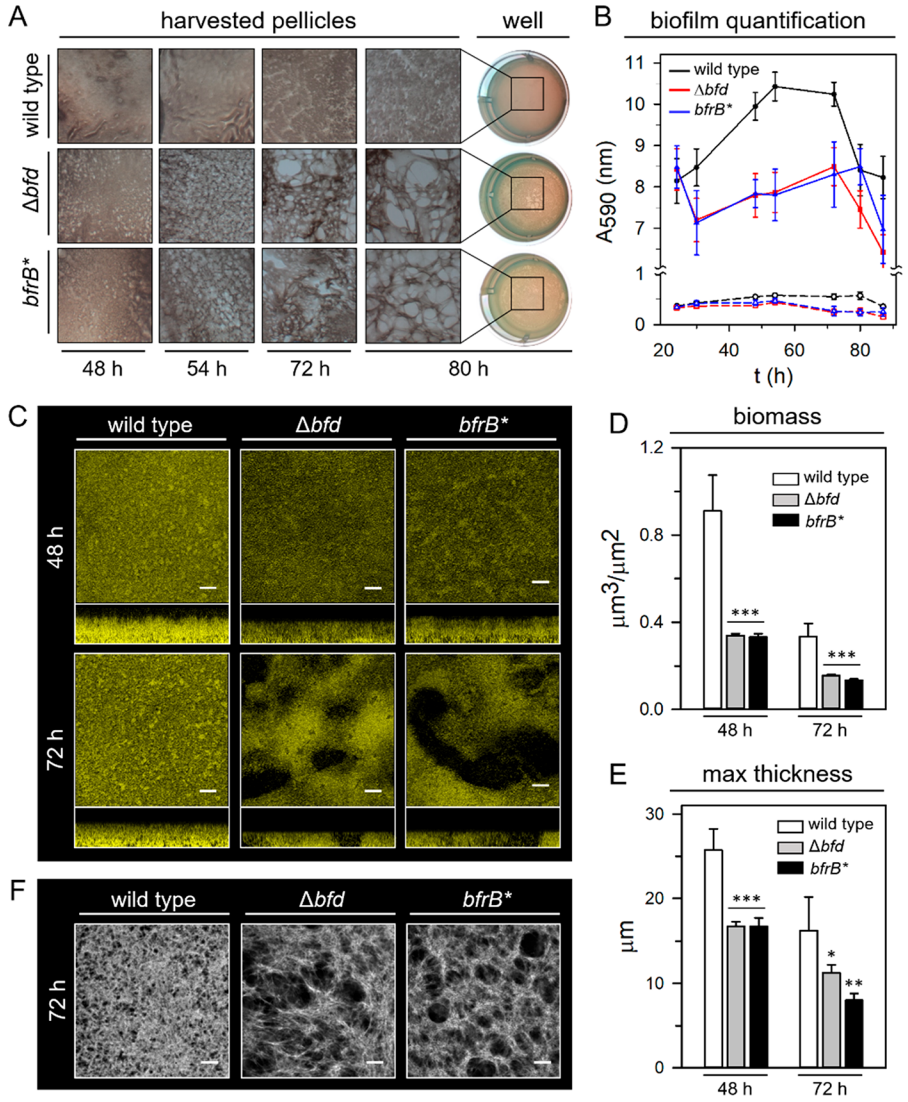

Figure 2. Blocking the BfrB-Bfd complex in *P. aeruginosa* cells impairs biofilm formation. (A) Photographs of pellicles harvested at different time points from static cultures in PI media supplemented with 20 μM Fe. To provide perspective, the column on the right shows photographs of the wells depicting the pellicles, while the remainder columns show photographs of the pellicles obtained with 10× magnification. (B) Time-dependent estimation of biofilm mass stained with crystal violet. The solid lines track biofilm mass in the pellicles, and the dashed lines track biofilm mass in the rings formed on the wells; note the break in the *y*-axis scale when the A_{590} is 1.0. Values are expressed as the mean of five independent cultures with standard deviations indicated by the error bars. (C) Maximum projection representation (squares) and vertical sections (rectangles) of CLSM images obtained from 2- and 3-day-old pellicles formed by cells expressing EYFP. (D) Biomass and (E) maximum thickness calculated with the aid of COMSTAT2 software. (F) Maximum projection representation of the extracellular matrix visualized by staining with the fluorescently labeled lectin ConA. The scale bars represent 20 μm. The *bfrB*(L68A/E81A) variant has been abbreviated *bfrB** for simplicity. $p < 0.05$ denoted by *, $p < 0.01$ by **, and $p < 0.001$ by *** relative to wild type.

violet staining, over a period of 87 h. The biofilm attached to the walls of the wells (rings) was also stained with crystal violet. The growth curves (Figure S1) show that the wild type and mutant cells exhibit similar rates of planktonic growth under the experimental culture conditions, transitioning from exponential to stationary growth phase ∼18 h post-inoculation. A thin film started to develop at the air−liquid interface at ∼12 h, which matured into an opaque pellicle *ca.* 48 h. As a first step in the characterization of these biofilms, the pellicles were dehydrated with methanol, harvested, and transferred to a clean well for washing with deionized water. Subsequent gentle removal of water from the wells allowed the dehydrated pellicles to settle at the bottom where they were photographed before staining with crystal violet. The photographs (Figure 2A) illustrate the robust pellicles that can be harvested from wild type cell cultures at 48 h post-inoculation; these pellicles remain nearly intact to approximately 72 h when the appearance of gaps suggests the beginning of pellicle dispersion. In contrast, the Δ*bfd* or *bfrB*(L68A/E81A) mutant cells form significantly less robust pellicles with noticeable gaps at 48 h which become considerably larger thereafter. It is also of note that as the pellicles formed by the mutant cells begin to disperse (∼54 h), these are no longer attached to the walls of the wells.

To obtain a more quantitative comparison of the differences in the pellicles formed by wild type and mutant *P. aeruginosa* cells, the harvested pellicles and the cells attached to the well walls were stained with crystal violet. The plots tracking the time-dependent intensity of the crystal violet absorbance at 590 nm (A_{590}) (Figure 2B) reveal three important findings: (*i*)

https://dx.doi.org/10.1021/acsinfecdis.9b00398
ACS Infect. Dis. 2020, 6, 447−458

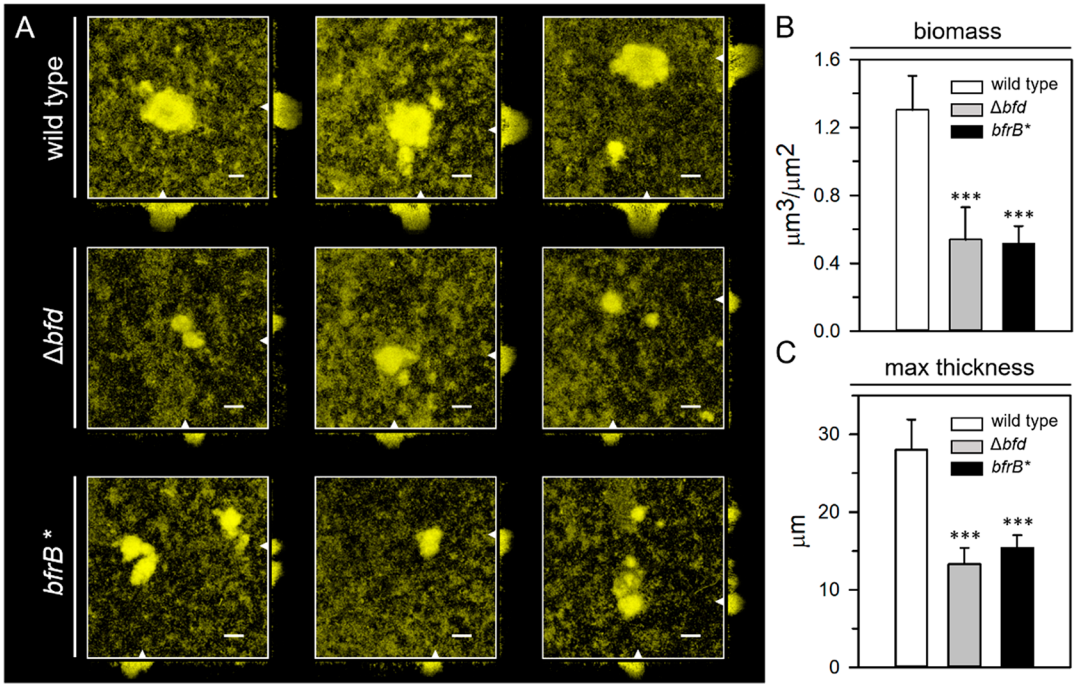

Figure 3. Blocking the BfrB-Bfd complex in *P. aeruginosa* impairs the maturation of surface biofilms grown in flow cells. (A) Four-day-old biofilms of wild type, Δ*bfd*, and *bfrB** cells expressing EYFP; representative images acquired at three different locations are shown. Maximum fluorescence projections are depicted with vertical sections (right and bottom) taken at the point represented by the white triangles. The scale bars represent 20 μm. (B) Biomass and (C) maximum biofilm thickness calculated with the aid of COMSTAT2 software. Values are averages of data from ten image stacks; error bars indicate standard deviation. The *bfrB*(L68A/E81A) variant has been abbreviated as *bfrB** for simplicity. $p < 0.001$ denoted by *** relative to wild type.

The majority of biofilm mass is contained within the pellicles, with only a small fraction of biofilm mass attached to the well walls (rings). (*ii*) Pellicles formed by wild type cells add biomass between 24 and 48 h, then remain relatively constant to approximately 72 h when biofilm mass is rapidly lost, presumably as a consequence of nutrient depletion in the culture media. (*iii*) At 24 h post-inoculation pellicles formed by the Δ*bfd* or *bfrB*(L68A/E81A) mutants contain approximately the same amount of biomass as the pellicles formed by the wild type cells. Beyond this point, however, the pellicles formed by the mutants do not add biofilm mass before the onset of rapid loss starts *ca.* 72 h. The large differences in the pellicles formed by wild type and mutant *P. aeruginosa* cells are also observed in images obtained with the aid of confocal laser scanning microscopy (CLSM) from pellicles formed by EYFP (enhanced yellow fluorescence protein) expressing strains harvested at 48 and 72 h (Figure 2C). The pellicles formed by the wild type cells are composed of a relatively uniform embedding of cells. In contrast, the pellicles obtained from the Δ*bfd* or *bfrB*(L68A/E81A) mutants are not uniform; the cells are not closely packed and there are significant gaps devoid of cells at 72 h. The COMSTAT2 software was used to attempt a quantitative comparison of the biomass (Figure 2D) and the maximum thickness of the pellicles (Figure 2E). The biomass in each of the pellicles was estimated from the biovolume, which is calculated as the overall pellicle volume/substratum area ($\mu m^3/\mu m^2$). In agreement with the observations made with the aid of crystal violet staining, the biomass associated with the pellicles formed by the wild type cells is ∼2-fold higher than that associated with the pellicles formed by the Δ*bfd* and *bfrB*(L68A/E81A) mutants. Consistent with these differences, the pellicles formed by the mutants are ∼50% thinner than those formed by their wild type counterpart. Cells in biofilms are embedded in a self-produced matrix of hydrated extracellular polymeric substances (EPS) composed mainly of polysaccharides, proteins and nucleic acids.[33] To observe the extracellular matrix in the pellicles, the polysaccharides containing terminal mannose and glucose moieties were stained with the fluorescently labeled lectin concanavalin A (ConA) and visualized with the aid of CLSM (Figure 2F). These experiments showed that the pellicles formed by the Δ*bfd* and *bfrB*(L68A/E81A) mutants exhibit spaces devoid of EPS matrix, similar to the spaces devoid of cells that are observed when imaging fluorescence emitted from EYFP-expressing cells (Figure 2C). Together, the images indicate that the pellicles formed by the mutant cells exhibit holes devoid of cells and matrix at 72 h.

Blocking the BfrB-Bfd Interaction in *P. aeruginosa* also Impairs Surface-Attached Biofilms. To determine if blockade of the BfrB-Bfd interaction in *P. aeruginosa* also has an adverse effect on the formation of biofilms grown on solid surfaces, we cultured biofilms of EYFP-expressing *P. aeruginosa* in flow cells. The results from these experiments are consistent with the observations made with the pellicle biofilms. Whereas the wild type cells formed cell clusters that matured into mushroom-like structures typically observed with *P. aeruginosa* (Figure 3A), the Δ*bfd* and *bfrB*(L68A/E81A) mutants formed significantly smaller and shallower structures. Analysis of 4-day-old CLSM biofilm images using COMSTAT2 showed that the biomass (Figure 3B) and the maximum thickness (Figure 3C) of the wild type biofilms are ∼2.5 times higher than in the biofilms formed by the mutant strains. Taken together, these observations strongly suggest that the iron homeostasis dysregulation caused by blocking the BfrB-Bfd interaction

https://dx.doi.org/10.1021/acsinfecdis.9b00398
ACS Infect. Dis. 2020, 6, 447−458

adversely affects the biofilm lifestyle of *P. aeruginosa* cells, either at air−liquid or solid−liquid interfaces.

Planktonic and Pellicle-Embedded Δ*bfd* and *bfrB*(L68A/E81A) Cells Exhibit Cytosolic Iron Deficiency. The above-described observations indicate that blocking the BfrB-Bfd complex in the *P. aeruginosa* cytosol causes iron homeostasis dysregulation, which in turn elicits an impaired biofilm maturation phenotype. To obtain a more direct correlation between iron homeostasis dysregulation and the biofilm maturation phenotype, it is necessary to monitor the intracellular iron levels of planktonic and biofilm-embedded cells, as well as iron concentrations in the culture media. As will be described below, these experiments allowed us to establish a correlation between cytosolic iron deficiency and the impaired biofilm formation phenotype exhibited by the Δ*bfd* and *bfrB*(L68A/E81A) mutants. These tasks were facilitated by studying pellicle biofilms because as shown above, pellicles can be readily harvested from their corresponding planktonic cell suspensions.

Analysis of iron concentrations in spent media used to grow pellicle biofilms indicated that the wild type and mutant cells deplete the iron from the culture media at very similar rates (Figure 4A). A fast phase lasting to ∼20 h post-inoculation is followed by a significantly slower phase, resulting in approximately 9 μM unused iron in the spent media at the end of the culture (∼72 h). It is therefore noteworthy that the significant concentration of iron left in the culture supernatants indicates that the failure of the Δ*bfd* and *bfrB*(L68A/E81A) cells to form robust pellicles is not a consequence of iron depletion in the growth media. In this context, it is remarkable that beyond 24 h post-inoculation the mutant cells secrete 4- to 7-fold more pyoverdine than the wild type cells (Figure 4B). The pronounced pyoverdine overproduction phenotype displayed by the mutants, which is typically associated with low iron conditions, is inconsistent with the relatively high levels of iron in the culture media. Rather, the observations are consistent with the mutant cells erroneously sensing severe iron limitation, probably due to the irreversible iron accumulation in BfrB and the cytosolic iron limitation ensuing upon blocking the BfrB-Bfd interaction.[12] The results from determinations of total intracellular and free intracellular iron levels in planktonic and pellicle-embedded cells support this idea (Figure 5). Free intracellular iron levels, also known as the labile iron pool,[34] is a measure of iron not stably incorporated into proteins, enzymes, or iron storage proteins, whereas total iron levels indicate the total content of intracellular iron, free and incorporated into macromolecules. To carry out these measurements, cells were cultured in Petri dishes, in order to obtain pellicles sufficiently large to provide the cell density required for whole-cell electron paramagnetic resonance (EPR) spectroscopic detection of intracellular free iron. The pellicles were harvested 48 h post-inoculation and the levels of free intracellular iron were measured as described in the Experimental Section using the cell-permeable Fe^{3+} chelator desferroxamine mesylate (DFO).[13,35] The relatively high affinity of DFO for Fe^{3+} facilitates the quantitative oxidation of free intracellular Fe^{2+} to form a Fe^{3+}-DFO chelate, which exhibits a sharp first derivative EPR signal with a *g*-value of 4.3 (Figure S2). The intracellular free iron content was quantified from the amplitude of this signal and a standard curve prepared from Fe^{3+}-DFO and normalized to the mass of protein present in the pellicle. To quantitate the intracellular free iron in the planktonic cells, these were collected by centrifugation immediately after removal of the pellicle. The harvested planktonic cells were treated with DFO and the intracellular free iron quantitated from the amplitude of the EPR signals at *g*

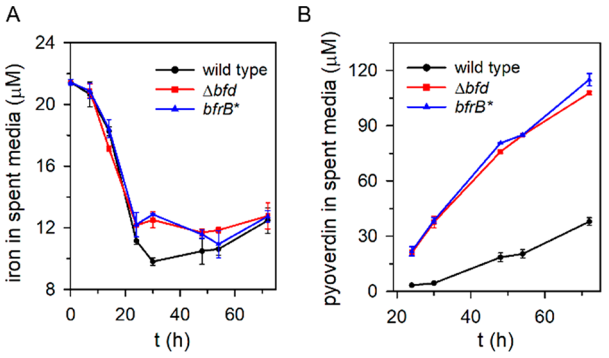

Figure 4. Blocking the BfrB-Bfd interaction in *P. aeruginosa* cells elicits a pyoverdine overproduction phenotype even in iron-replete conditions. (A) Time-dependent concentrations of iron in the culture media used to grow the pellicles. (B) Concentrations of pyoverdine secreted by wild type, Δ*bfd*, and *bfrB**. Each of the points in the plots indicates the mean and standard deviation from five replicates of a representative experiment. The *bfrB*(L68A/E81A) variant has been abbreviated as *bfrB** for simplicity.

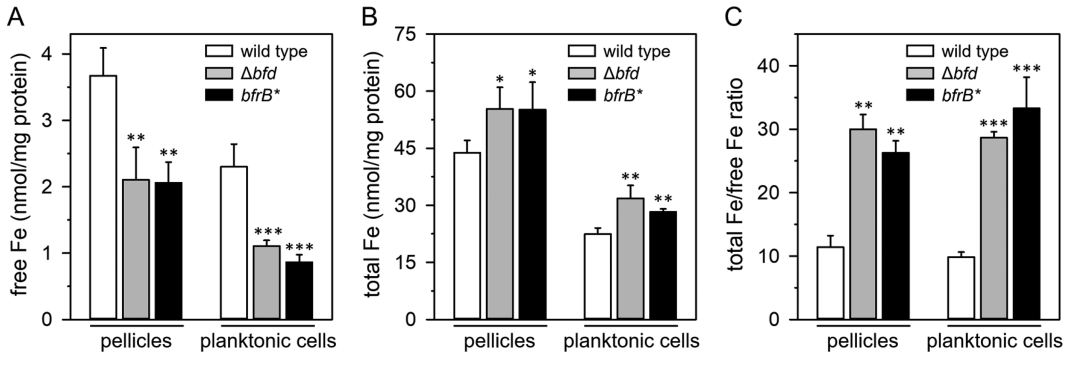

Figure 5. Blocking the BfrB-Bfd interaction causes a cytosolic iron deficiency in planktonic and pellicle-embedded cells. Levels of (A) free intracellular and (B) total intracellular iron in wild type, Δ*bfd*, and *bfrB** cells in the planktonic or pellicle-embedded lifestyle measured 48 h post-inoculation. (C) Wild type cells display a ratio of total Fe/free Fe of ∼10; the 3-fold larger ratio in the mutants is indicative of iron homeostasis dysregulation. The *bfrB*(L68A/E81A) variant has been abbreviated as *bfrB** for simplicity. $p < 0.05$ denoted by *, $p < 0.01$ by **, and $p < 0.001$ by *** relative to wild type.

https://dx.doi.org/10.1021/acsinfecdis.9b00398
ACS Infect. Dis. 2020, 6, 447−458

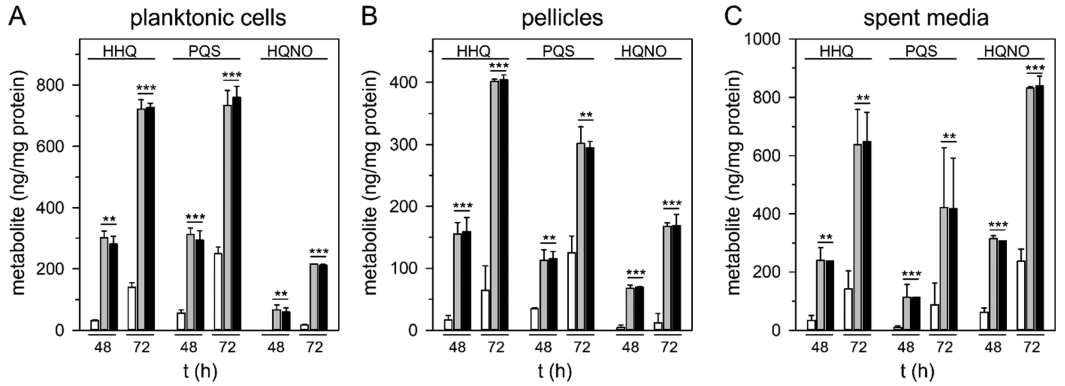

Figure 6. Blocking the BfrB-Bfd complex in *P. aeruginosa* elicits a 2-alkyl-4-quinolone (AQ) hyperproduction phenotype. LC-MS-determined levels of HHQ, PQS, and HQNO in (A) planktonic cells, (B) pellicles, and (C) spent media of wild type (white), Δ*bfd* (gray), and *bfrB*(L68A/E81A) (black) cell cultures normalized to the corresponding total mass of protein; the mass of AQs in spent media was normalized to the total mass of protein in the planktonic cells and pellicles. Cells were cultured statically in PI media supplemented with 20 μM Fe for 48 or 72 h. Means and standard deviations from triplicate experiments are shown. $p < 0.01$ denoted by **, and $p < 0.001$ by *** relative to wild type.

= 4.3 and then normalized to the mass of protein present in the cell pellet.

The results show that the levels of intracellular free iron in the Δ*bfd* or *bfrB*(L68A/E81A) mutant cells are approximately 50% of those in the wild type cells, both in the planktonic and in the pellicle-embedded cells (Figure 5A). In contrast, the levels of total intracellular iron in the mutant cells, planktonic or embedded in pellicles, are approximately 150% of those of the wild type cells (Figure 5B). It is also instructive to consider the ratios of total intracellular Fe/free intracellular Fe (Figure 5C). This comparison makes it evident that in the wild type cells, whether in planktonic or sessile state, iron homeostasis is indicated by a total Fe/free Fe ratio of approximately 10. These ratios in the Δ*bfd* and *bfrB*(L68A/E81A) mutant cells are approximately 30, thus clearly indicating iron homeostasis dysregulation caused by accumulation of unusable trapped iron in BfrB and by low free cytosolic iron. Taken together, these observations demonstrate that blockade of the BfrB-Bfd interaction results in the irreversible accumulation of iron in BfrB and concomitant iron deficiency in the cytosol. It is important to underscore that the intracellular deficiency of free iron in the mutant cells (Figure 5A) occurs despite the significant amounts of unused iron (~9 μM) left in the culture media (see Figure 4A). Consequently, it is reasonable to conclude that blocking the BfrB-Bfd interaction causes intracellular iron deficiency which results in the cells erroneously sensing environmental iron limitation and responding by deploying iron procuring systems (e.g., pyoverdine) and possibly signaling biofilm dissolution. Finally, it is also interesting to note that the levels of free and total intracellular iron in pellicle-embedded cells are nearly twice the corresponding iron levels in the planktonic cells. These observations, which represent the first quantitative comparison of iron requirements in biofilm and planktonic cells, support the idea that biofilm-embedded cells have a higher iron requirement than their planktonic counterparts.[36]

Blocking the BfrB-Bfd Interaction Stimulates the *Pseudomonas* Quinolone Signal (PQS) Pathway. Iron homeostasis in *P. aeruginosa* depends on an intricate regulatory cascade that controls the expression of iron uptake systems in response to intracellular iron levels. These systems are controlled by the master ferric uptake regulator (Fur), an iron-binding transcriptional repressor that blocks the transcription of iron uptake systems such as those involved in the biosynthesis of the siderophores pyoverdine and pyochelin.[37,38] Hence, the pyoverdine hyperproduction phenotype exhibited by the Δ*bfd* and *bfrB*(L68A/E81A) cells (Figure 4B) is in agreement with the low levels of intracellular free iron in the mutants relative to the wild type cells (Figure 5A). Low iron conditions are also known to stimulate the biosynthesis of 2-alkyl-4-quinolones (AQs), such as the *Pseudomonas* quinolone signal PQS (2-heptyl-3-hydroxy-4-quinolone), HHQ (2-heptyl-4-hydroxyquinoline), and HQNO (2-heptyl-4-hydroxyquinoline-*N*-oxide), which involves the condensation of fatty acid and anthranilate. Conditions of iron limitation stimulate the biosynthesis of AQs via two main regulatory cascades involving the PqsR transcription factor (also known as MvfR) and the sibling small regulatory RNAs PrrF1 and PrrF2: (*i*) PqsR is induced by PQS and HHQ, and is also stimulated by the iron starvation σ factor PvdS.[39] PqsR in turn controls the *pqsABCDE* operon,[40] whose gene products direct the synthesis of AQs,[41,42] which mediate important biological activities including quorum sensing. (*ii*) The biosynthesis of AQs is also stimulated by the Fur-regulated sRNAs PrrF1 and PrrF2.[42,43] The PrrF sRNAs, transcribed in response to iron limiting conditions, among other processes, repress genes coding for enzymes that catalyze anthranilate degradation (*antABC* and *catBCA*), thus sparing anthranilate for the biosynthesis of AQs.[41,44] Consequently, we anticipated that dysregulation of iron homeostasis by blocking of the BfrB-Bfd interaction, which leads to an iron deficiency in the cytosol, should also stimulate production of AQs. To test this idea, we utilized HPLC-tandem mass spectrometry to quantitate the AQs present in the pellicles and in the planktonic cells at 48 and 72 h post-inoculation (Figure S3). To facilitate comparison among different strains, the mass of AQs was normalized to protein mass (Figure 6). These experiments showed that in the planktonic cells and in the pellicles formed by the Δ*bfd* and *bfrB*(L68A/E81A) mutants the levels of HHQ, PQS, and HQNO are approximately 10-fold larger than the levels detected in the corresponding samples of wild type cells (Figure 6A and B). Quantitative analysis of AQs in the spent media (Figure 6C) showed a similar trend, with AQ levels ~5-fold larger in spent media samples from Δ*bfd* and *bfrB*(L68A/E81A) cell cultures relative to samples obtained from wild type cells. These observations are in excellent

https://dx.doi.org/10.1021/acsinfecdis.9b00398
ACS Infect. Dis. 2020, 6, 447−458

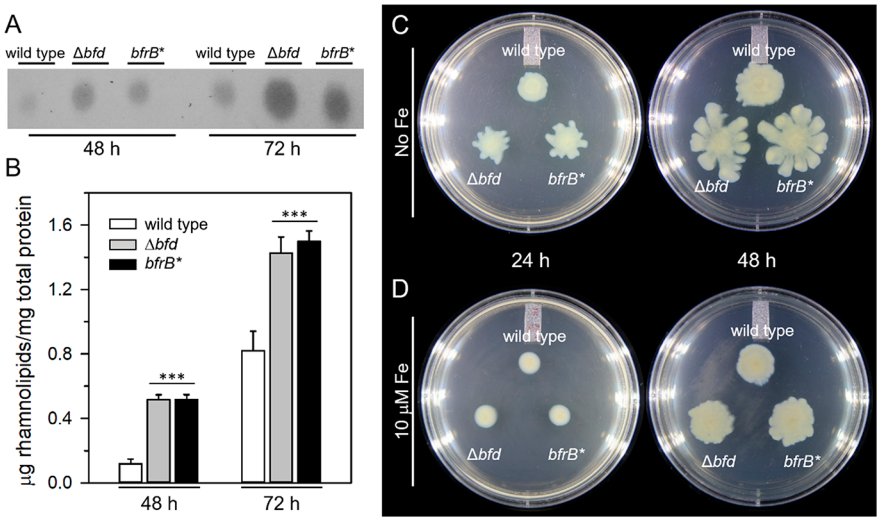

Figure 7. Blocking the BfrB-Bfd interaction results in enhanced rhamnolipid production and swarming motility. Rhamnolipids extracted into ethyl acetate from acidified cell-free supernatant solutions were visualized in (A) TLC plates and (B) quantitated using methylene blue and normalized to mass of protein. Cells were cultured under static conditions for 48 and 72 h in PI media supplemented with 20 μM Fe. The data represent averages from three independent experiments and the error bars indicate the standard deviations. (C) Swarming plates not supplemented and (D) supplemented with 10 μM Fe were inoculated with wild type, Δ*bfd*, and *bfrB** cells and incubated at 37 °C for 24 and 48 h. The *bfrB*(L68A/E81A) variant has been abbreviated as *bfrB** for simplicity. $p < 0.001$ denoted by *** relative to wild type.

agreement with the expectation that the low levels of intracellular free iron in the mutants caused by blocking of the BfrB-Bfd complex elicit an AQs hyperproduction phenotype.

Blocking the BfrB-Bfd Interaction Enhances Rhamnolipid Synthesis and Induces Swarming Motility. The observations presented so far indicate that blocking the BfrB-Bfd complex elicits cytosolic iron limitation which causes the mutant cells to erroneously sense iron limitation and in response mount an iron starvation response, as demonstrated by the overproduction of pyoverdine and AQs, despite sizable iron levels remaining in the culture media. The cytosolic iron deficiency that results from blocking the BfrB-Bfd interaction also elicits a biofilm-deficient phenotype, observations that are in excellent agreement with previous reports demonstrating that environmental iron limitation, for example, by the addition of lactoferrin or iron chelating agents, increases surface motility, inhibits biofilm maturation,[16] and encourages transition to the planktonic lifestyle.[45] In this context, rhamnolipids are recognized as important for defining the structure of *P. aeruginosa* biofilms.[46] Under iron replete conditions, rhamnolipids are produced in the late stages of biofilm formation. Conditions of iron limitation, on the other hand, are known to shift the timing of rhamnolipid expression to the earlier stages of biofilm formation, which results in increased bacterial surface motility,[36,47,48] most notably, swarming motility[49−51] and biofilm dispersal.[52] Rhamnolipid synthesis is under control of the *rhlAB* operon, which is induced under the conditions of iron limitation,[47] and is also regulated by the RhlI/R quorum sensing system.[50,53,54] It is also significant that the biosynthesis of rhamnolipids and PQS share the common precursor β-keto-decanoic acid[55] and that rhamnolipids increase the solubility and bioactivity of PQS.[56] Hence, the cytosolic iron limitation ensuing in the Δ*bfd* and *bfrB*(L68A/E81A) mutants, which elicits PQS overproduction and deficiencies in biofilm maturation, led us to hypothesize that the mutants should also overproduce rhamnolipids compared with the wild type cells. Analysis of rhamnolipids in spent media corroborated this idea (Figure 7A and B): the Δ*bfd* and *bfrB*(L68A/E81A) cells secrete ∼5-fold higher levels of rhamnolipids than the wild type cells at 48 h and ∼2-fold higher levels at 72 h. These observations are in good agreement with the expectation that the cytosolic iron limitation experienced by the mutant cells shift the timing of rhamnolipid biosynthesis to the earlier stages of biofilm formation. The increased levels in both mutant strains and the smaller differences between wild type and mutant cultures observed at 72 h are also consistent with the accelerated pellicle dissolution that takes place beyond 72 h in the cultures of all three strains (see Figure 2). Therefore, it is reasonable to conclude that the early production of rhamnolipids by the mutants, which is very likely a consequence of cytosolic iron limitation imposed by blocking the BfrB-Bfd complex, is probably an important determinant for the inability of the mutants to form mature pellicles, even under iron replete conditions (see Figure 2). We surmise that similar circumstances prevent the Δ*bfd* and *bfrB*(L68A/E81A) mutant cells from forming mature (mushroom shape) biofilms in the flow cells (Figure 3).

Iron availability strongly influences the inverse relation between swarming and biofilm formation. Iron limitation induces motility and transition to the planktonic lifestyle, while iron replete conditions facilitate biofilm formation.[45,47] Given the early production of rhamnolipids by the mutants and the direct relationship between rhamnolipid production, surface motility, and biofilm dispersion, we also compared the surface motility of the Δ*bfd* and *bfrB*(L68A/E81A) mutants to that of the wild type cells. The results from these experiments show that blocking the BfrB-Bfd interaction promotes *P. aeruginosa* swarming motility (Figure 7C). In comparison, when the agar plates are supplemented with 10 μM Fe, the swarming phenotype of the Δ*bfd* and *bfrB*(L68A/E81A) cells is significantly attenuated (Figure 7D), supporting the idea that the mutants sense iron limitation earlier than their wild type counterparts as a consequence of the irreversible trapping of iron in BfrB and concomitant iron deficiency in the cytosol. No

https://dx.doi.org/10.1021/acsinfecdis.9b00398
ACS Infect. Dis. 2020, 6, 447−458

differences were observed in swimming motility between the wild type and mutant cells (Figure S4).

Concluding Remarks. Although iron is essential for bacteria due to its involvement in fundamental cellular processes, the nutrient can present cells with the problems of toxicity and solubility. Consequently, bacterial iron metabolism depends on intact iron homeostasis machinery to satisfy the nutritional requirement while preventing iron-induced toxicity. Our previous work has shown that iron homeostasis in *P. aeruginosa* depends on the ability of Bfd to bind to BfrB and promote the mobilization of BfrB-stored iron to establish a dynamic equilibrium between cytosolic $Fe^{2+}$and Fe^{3+} in BfrB, which functions to buffer Fe^{2+} in the range of concentrations required to enable the Fur-regulated process of iron acquisition and utilization.[12] An important consequence of blocking the BfrB-Bfd complex in *P. aeruginosa* is inhibition of iron mobilization from BfrB and loss of the dynamic equilibrium that buffers cytosolic Fe^{2+} concentrations, ultimately inducing cytosolic iron deficiency.[12] Hence, the work reported herein departed from the premise that the cytosolic iron deprivation induced by preventing the BfrB-Bfd association would exert a detrimental effect on the biofilm lifestyle of *P. aeruginosa*, since it is well-known that biofilm maturation requires iron replete conditions.[8,17] An important concept supported by this work is that the cytosolic iron deprivation induced by blocking the BfrB-Bfd complex occurs irrespective of the iron concentration in the culture media (environmental iron). Thus, iron starvation conditions can be established in the absence of iron chelators and irrespective of the iron concentration in the environment. The iron starvation response, in turn, elicits defects in biofilm formation, which are evident in the data (Figures 2 and 3) showing that the pellicles and surface biofilms formed by the Δ*bfd* and *bfrB*(L68A/E81A) mutant cells are significantly less well developed than biofilms formed by the wild type cells under identical iron-replete culture conditions. Experiments with pellicle biofilms demonstrate that the mutants overproduce pyoverdine, despite having access to sufficient environmental iron (Figure 4). The cytosolic iron deprivation experienced by the mutants, which is strongly suggested by the pyoverdine overproduction phenotype, has been corroborated in the measurements of intracellular total and free iron (Figure 5). These measurements indicate that planktonic and pellicle-embedded mutant cells have lower concentrations of cytosolic free iron than the wild type cells. The measurements also provide quantitative evidence that biofilm-associated *P. aeruginosa* cells have higher iron levels than their planktonic counterparts. Iron starvation in the mutant cells also stimulates an overproduction of AQs and a shift in the timing of rhamnolipid biosynthesis to earlier phases of biofilm formation. These phenotypes are consistent with the well-known effect of low environmental iron on inducing rhamnolipid biosynthesis, swarming motility, and biofilm dispersion.[47−50] Consequently, it is reasonable to conclude that the cytosolic iron deficiency caused by blocking the BfrB-Bfd complex discourages the biofilm lifestyle, even in iron-sufficient conditions, which are typically conducive to biofilm formation. In this context, it is noteworthy that alignment of the *P. aeruginosa* BfrB and Bfd sequences against Bfr and Bfd sequences from *E. coli 0157*, *Klebsiella pneumoniae*, *Yersinia pestis*, *Shigella dysenteriae*, *Enterobacter sp.*, and *Acinetobacter baumannii* shows that the key residues participating at the interface of the BfrB-Bfd complex in *P. aeruginosa* are conserved in the Bfr and Bfd sequences of the above-listed pathogens.[28,30] This suggests that the repercussions of inhibiting the Bfr-Bfd interaction reported here for *P. aeruginosa* are of widespread significance.

EXPERIMENTAL SECTION

Bacterial Strains. *Pseudomonas aeruginosa* PAO1-UW[57] was purchased from the University of Washington Genome Center. The PAO1-derived strains with unmarked, in-frame deletion of the *bfd* gene (Δ*bfd*) or harboring the L68A/E81A double mutant *bfrB* allele [*bfrB*(L68A/E81A] had been previously prepared.[12] *P. aeruginosa* strains were fluorescently tagged with EYFP (Enhanced Yellow Fluorescent Protein) at the unique and neutral *att* site using the mini-Tn7 transposon system described previously.[58] The delivery plasmid pUC18T-mini-Tn7T-Gm-eyfp (plasmid # 65031, Addgene) was introduced in *P. aeruginosa* cells by electroporation and the gentamicin resistance marker was removed from the genome using pFLP2.[59]

Media and Growth Conditions. Pseudomonas Isolation (PI) media (20 g L^{-1} peptone, 0.3 g L^{-1} $MgCl_2{\cdot}6H_2O$, 10 g L^{-1} K_2SO_4, 25 mg L^{-1} irgasan, and 20 mL L^{-1} glycerol, pH 7.0) was used for normal growth conditions. For all experiments, starter cultures were grown from a single colony at 37 °C and shaking at 220 rpm for 16 h in 5 mL PI media supplemented with 10 μM iron. Pellicle biofilm growth experiments were carried out at 30 °C in PI broth supplemented with 20 μM Fe. Surface attached biofilms were grown in AB media[60] supplemented with trace metals (0.15 μM ammonium molybdate, 3 μM $CuSO_4$, 2 μM $Co(NO_3)_2$, 9.4 μM $Na_2B_4O_7$, and 7.6 μM $ZnSO_4$), 3 mM glucose and 15 μM Fe. Iron supplementation was carried out by addition of a small volume of filter-sterilized solution of 10 mM $(NH_4)_2Fe(SO_4)_2$ (pH ∼2.0).

Growth Curves. Changes in the size of planktonic cell population over time in statically grown cultures were obtained in separate experiments by drawing 100 μL samples of liquid culture from the microplate wells, serially diluting in PBS (pH 7.4), plating on PI agar (Bacto) plates, incubating 16 h at 37 °C, and enumerating colony forming units per mL (CFU/mL).

Biofilm Growth at the Air−Liquid Interface. Pellicle biofilms were grown in tissue culture treated 24-well polystyrene microplates (Fisher). Starter cultures were diluted to an optical density at 600 nm (OD_{600}) of 0.001 in 1.5 mL of PI media supplemented with 20 μM Fe, deposited in the microplate wells and incubated at 30 °C without shaking. The total amount of biofilm (pellicle at the air−liquid interface and "ring" of cells attached to the wells) was quantified by the crystal violet assay.[61] To stain the pellicles, 500 μL of methanol was gently layered on top of each pellicle to dehydrate and rigidify it.[31] The dehydrated pellicles were harvested with a looped wire and transferred to clean wells containing 1 mL deionized water. The water was removed, allowing the pellicles to settle at the bottom of the wells, where they were photographed using a Nikon SMZ-2T microscope and a Cannon E0S 1300D (W) camera. The pellicles were air-dried and then stained with slow shaking for 1 h in 2 mL of 0.1% crystal violet solution (Aqua Solutions). After washing two times with deionized water, the crystal violet was solubilized by adding 2 mL 30% acetic acid and incubating 3 h at ambient temperature with slow shaking. The absorbance at 590 nm was measured in an Epoch 2 microplate spectrophotometer (BioTek). The "ring" biofilms attached to the walls of the

https://dx.doi.org/10.1021/acsinfecdis.9b00398
ACS Infect. Dis. 2020, 6, 447−458

culture wells were stained with crystal violet as described above after removal of the pellicles and the spent media.

Confocal Laser Scanning Microscopy of Pellicles. *P. aeruginosa* cells expressing EYFP were statically grown at 30 °C for 48 and 72 h in 35 × 10 mm Petri dishes containing 4 mL PI media supplemented with 20 μM Fe. The pellicles were transferred onto circular (1.5 cm diameter) glass coverslips by gently allowing the surface of a coverslip to come into contact with a pellicle. The pellicle-adhered coverslips were washed in PBS, mounted on glass slides using 10 μL SlowFade (Life Technologies), and the edges sealed with fingernail polish. To visualize the extracellular matrix the pellicle-adhered coverslips were stained by dipping in 500 μL of PBS containing 300 μg/mL concanavalin A (conA) conjugated with Alexa Fluor 647 (Life Technologies) for 30 min. Excess fluorescent dye was washed with PBS and the coverslip was mounted on a glass slide as described above. CLSM images were acquired with the aid of a Leica TCS SP8 microscope (Leica Microsystems, Germany) using a HC PL apo CS2 63×/1.4 oil objective. For detecting the EYFP fluorescence the laser line was set at 506 nm and the emission range to 511−778 nm. Alexa Fluor 647 fluorescence was detected with excitation at 653 nm and emission range 658−701 nm. Image stacks were acquired with a *z*-step size of 0.3 μm. The Leica Application Suite X (LAS-X) software was used for image stack processing. Quantitative analysis was performed using the COMSTAT2 computer program.[62] The pellicle biomass and maximum thickness were determined with a manual thresholding set at 170 and 200 for images acquired at 48 and 72 h, respectively.

Flow Cell Biofilm Assay. Surface-attached biofilms of *P. aeruginosa* cells expressing EYFP were grown on flow cells with an 800 μm channel depth (μ-slide $I^{0.8}$ Luer, Ibidi) using an automated perfusion system (Ibidi, Munich, Germany). The flow cell was inoculated with 200 μL of an overnight culture diluted to OD_{600} = 0.5, followed by 1 h incubation at 30 °C to allow bacterial cell attachment. The μ-slide was connected to the Ibidi Pump System and the biofilms were cultured for 4 days at 30 °C while flowing AB media. The experimental shear stress was 0.14-dyn/cm^2 (shear rate = 14 s^{-1}, pressure = 7.1 mbar, flow rate = 0.4 mL/min) and the switch time was set to 540 s. The culture medium in the reservoirs was removed every 12 h and replaced with fresh prewarmed medium. The biofilms were imaged with the aid of CLSM as described above. Z-series images were taken in 0.3 μm slices at different positions of the μ-slide. Vertical cross sections and projections were generated using the LAS-X software package. Quantitative analysis of biofilm biomass and maximum thickness was performed with the COMSTAT2 computer program[62] using the Otsu method of automatic thresholding.[63]

Analysis of Pyoverdine. Pyoverdine secreted to the spent media of the statically grown cultures was analyzed in 1.5 mL of cell culture withdrawn from each of the wells. The samples were centrifuged for 5 min at 12,500 rpm, followed by transfer of 1 mL of the supernatant to a glass tube for subsequent extraction of pyocyanin with 1 mL of chloroform. The aqueous and organic layers were separated by centrifugation and the UV−vis spectrum of the aqueous pyoverdine solution was obtained with the aid of Cary60 Bio UV−vis spectrophotometer. The concentration of pyoverdine was calculated from the absorbance intensity at 400 nm and the reported extinction coefficient (20 mM^{-1} cm^{-1}).[64]

Iron in Spent Media. The time-dependent concentration of iron in the culture media of statically grown pellicles was determined spectrophotometrically.[65] Samples (1 mL) were removed from the 24-well plates and centrifuged at 12,500 rpm for 5 min. The cell free supernatant (650 μL) was treated with 250 μL of iron-releasing reagent (0.6 N HCl, 2.25% (w/v) $KMnO_4$) and incubated at 65 °C for 3 h. The samples were cooled to ambient temperature, treated with 100 μL of iron detection reagent (6.5 mM ferrozine, 13.1 mM neocuproine, 2 M ascorbic acid, 5 M ammonium acetate), and incubated at ambient temperature (30 min). After centrifugation (5 min at 12,500 rpm), the absorbance of the Fe^{2+}-ferrozine complex at 562 nm was measured, and the iron concentration calculated using the reported extinction coefficient (27.9 mM^{-1} cm^{-1}).[66]

Intracellular Iron Levels. Levels of free intracellular iron in planktonic and pellicle-embedded cells were measured at 48 h using a previously reported whole-cell EPR spectroscopy method.[12,13] For analysis of pellicles, each of the strains was cultured statically at 30 °C in three Petri dishes (60 × 15 mm) containing 10 mL PI media supplemented with 20 μM Fe. The planktonic cells were removed by pipetting the culture media, allowing the pellicles to settle at the bottom of the Petri dishes. The three pellicles/strain were pooled, washed twice with 2 mL of PBS (pH 7.4), transferred to 15 mL conical tubes, and then centrifuged for 15 min at 4000 rpm and 4 °C. The cells were suspended in 5 mL ice-cold PI media containing 10 mM DTPA, incubated 5 min at ambient temperature prior to the addition of the intracellular iron chelator desferroxamine mesylate (DFO; 20 mM final concentration) and incubated for 10 min at 37 °C and 220 rpm. The cells were centrifuged and washed, once in 5 mL ice-cold PBS (pH 7.4), and once in 5 mL ice-cold deionized water. Finally, 200 μL of ice-cold PBS (pH 7.4) containing 10% glycerol was added to the cell pellet, followed by loading 200 μL of the cell slurry onto a 4 mm quartz EPR tube and immediately freezing by immersing the tube in a dry ice/acetone bath. The remaining slurry was frozen at −80 °C and used later to analyze the total levels of intracellular iron, as described below. A similar procedure was used to prepare the planktonic cells for whole-cell EPR spectroscopy. EPR spectra were recorded on a Bruker EMX spectrometer equipped with a standard ER-4102 resonator and an Oxford ESR-900 helium flow cryostat at 7.5 ± 0.5 K. The microwave frequency was 9.47 GHz, the microwave power was 2 mW, the modulation frequency was 100 kHz, the modulation amplitude was 20 G, the sweep time was 42 s, the conversion time was 20.5 ms, and the time constant was 164 ms. A standard curve was generated using identical parameters and solutions containing 0, 5, 10, 15, 20, and 25 μM Fe (from $Fe_2(SO_4)_3{\cdot}7H_2O$) and 2 mM DFO in 20 mM Tris-HCl buffer (pH 7.4) containing 10% glycerol. Total levels of intracellular iron were measured using a published method.[12,67] The cell pellets were thawed at ambient temperature, and 250 μL of the suspension was treated with 500 μL of freshly prepared iron releasing reagent, mixed by vortexing, and then incubated at 65 °C for 4 h. The resultant solutions were cooled to ambient temperature, treated with 100 μL of iron detection reagent, incubated for 30 min at ambient temperature, and centrifuged for 5 min at 12,500 rpm. The iron concentration was measured as described above and reported as Fe atoms per mg protein.

Determination of Protein Content. Planktonic or pellicle-embedded cell pellets were suspended in 400 μL PBS (pH 7.4) containing 50 mM NaOH and incubated at ambient temperature for 4 h with shaking, followed by neutralization by addition of HCl to a final concentration of 5 mM. The amount of protein was determined by the bicinchoninic acid method

https://dx.doi.org/10.1021/acsinfecdis.9b00398
ACS Infect. Dis. 2020, 6, 447−458

(BCA assay kit, Pierce) using bovine serum albumin as standard, following the manufacturer's instructions.

Analysis of 2-Alkyl-4-quinolones (AQs). HHQ, PQS, and HQNO extracted from pellicles, planktonic cells, and bacterial culture supernatants were quantified by liquid chromatography−mass spectrometry (LC-MS).[68] To this end, pellicles were grown statically at 30 °C for 48 or 72 h in 35 × 10 mm Petri dishes containing 4 mL PI media supplemented with 20 μM Fe. The AQs were extracted from bacterial cell pellets by resuspension in 1 mL of 100% methanol, as well as from 3 mL of spent media acidified with 15 μL of 12 N HCl into 6 mL of ethyl acetate. After 1 h incubation with slow shaking at room temperature, the organic layer was separated by centrifugation (1 min at 12,500 rpm), transferred to a new microcentrifuge tube and evaporated in a Savant SPD111 V SpeedVac concentrator. Dried samples were suspended in methanol (300 μL) and stored at −20 °C. Quantitative analysis of the AQs was performed with the aid of an LC-MS system comprising an Agilent 1260 Infinity II HPLC and an Agilent 6230 time-of-flight mass spectrometer operating in positive ion mode with a capillary voltage of 4000 V, end plate voltage of 150 V, and nebulizing gas (N_2) temperature of 325 °C. Samples were separated in a Poroshell 120 EC-C8 column (3.0 × 100 mm, 2.7 μm particle size, 120 Å pore size; Agilent) using a flow rate of 0.4 mL/min and the following gradient: 97% A (2 min), 63% A (5 min), 57% A (21 min), and 3% A (31 min), after which the gradient was reverted to the initial conditions and the column re-equilibrated for 11 min. Mobile phase composition was as follows: A: 0.1% formic acid in water. B: 0.1% formic acid in acetonitrile. AQs were detected using full scan mode (m/z 130 to 350) and quantitated by measuring the integrated peak area of the corresponding $[M + H]^+$ ions and a standard curve constructed from commercially available HHQ, HQNO, and PQS. The mass of AQs was normalized to the total amount of protein.

Analysis of Rhamnolipids. Pellicles were grown statically at 30 °C for 48 or 72 h in 35 × 10 mm Petri dishes containing 4 mL of PI media supplemented with 20 μM Fe. Rhamnolipids were extracted from 3 mL of cell-free supernatants acidified with 15 μL 12 N HCl into 6 mL of ethyl acetate by incubating at room temperature for 1 h with shaking. The organic phase (1.5 mL) was collected, evaporated to dryness in a SpeedVac concentrator, and the rhamnolipids quantitated using the methylene blue complexation method[69] and normalized to the total amount of protein. Briefly, dried rhamnolipids were dissolved in 300 μL of chloroform, followed by addition of 150 μL of freshly prepared aqueous methylene blue solution (400 μL of the 10 g/L methylene blue reagent, 9.6 mL of deionized water). After vigorous mixing, the samples were incubated at ambient temperature for 1 h with shaking. The absorbance of the chloroform phase was measured at 638 nm against a chloroform blank, and the absorbance values were converted to rhamnolipid concentrations using a calibration curve established by applying the same procedure to standard rhamnolipid (AGAE Technologies) solutions dissolved in PI media. For thin-layer chromatography (TLC) analysis, dried rhamnolipids were dissolved in 20 μL of methanol, and 2 μL of the resultant solution was spotted on a TLC silica gel 60 F_{254} plate (Millipore), previously impregnated with phosphate and activated for 1 h at 100 °C; 2 μg of the rhamnolipid standard (AGAE Technologies) was loaded to determine rhamnolipid electrophoretic mobility. The TLC plates were developed using chloroform/methanol/acetic acid (65:15:2), and then stained by immersion in detection agent solution for 2 min (0.15 g orcinol, 8.2 mL 60% sulfuric acid, and 42 mL water), air-dried at ambient temperature and then incubated at 110 °C for 10 min.[70]

Swarming Motility Assay. Swarming motility was investigated on soft agar plates containing 20 mL/plate of 0.8% (w/v) terrific broth, 0.5% (w/v) glucose, and 0.5% (w/v) agar.[71] A single colony of each strain was gently stabbed on the agar surface using a toothpick and the plates were incubated at 37 °C for 24 or 48 h prior to photographic documentation. To analyze the influence of iron on swarming motility, the media was supplemented with 10 μM Fe. Each experiment was carried out three times with at least three replicates for each bacterial strain.

Statistical Analysis. Statistical significance between the means and standard deviation of values obtained in experiments comparing wild type with the Δ*bfd* and *bfrB*(L68A/E81A) mutant strains was determined using one-way ANOVA followed by Tukey's multiple *post hoc* test, with the aid of SigmaPlot. Values of $p < 0.05$ are denoted by *, $p < 0.01$ by **, and $p < 0.001$ by ***.

■ ASSOCIATED CONTENT

Supporting Information

The Supporting Information is available free of charge at https://pubs.acs.org/doi/10.1021/acsinfecdis.9b00398.

> Growth curves of wild type, Δ*bfd*, and *bfrB*(L68A/E81A) mutant cells; whole-cell EPR spectra; mass spectral data for AQs determination; and swimming motility assays (PDF)

■ AUTHOR INFORMATION

Corresponding Author

Mario Rivera − *Louisiana State University, Baton Rouge, Louisiana;* orcid.org/0000-0002-5692-5497; Email: mrivera@lsu.edu

Other Authors

Anabel Soldano − *Louisiana State University, Baton Rouge, Louisiana*

Huili Yao − *Louisiana State University, Baton Rouge, Louisiana*

Josephine R. Chandler − *University of Kansas, Lawrence, Kansas;* orcid.org/0000-0001-8944-9813

Complete contact information is available at: https://pubs.acs.org/10.1021/acsinfecdis.9b00398

Author Contributions

A.S.: Pellicle and surface biofilm studies, quantitative analysis of iron and metabolites, construction of EYFP-expressing *P. aeruginosa* strains, and CLSM experiments. H.Y.: Initial work with pellicle biofilms and whole cell EPR analysis of free cytosolic iron. J.R.C.: Oversaw construction of EYFP expressing *P. aeruginosa* strains. M.R.: directed biology and analytical chemistry. A.S. and M.R. wrote the manuscript. H.Y. and J.R.C. edited the manuscript.

Notes

The authors declare no competing financial interest.

https://dx.doi.org/10.1021/acsinfecdis.9b00398
ACS Infect. Dis. 2020, 6, 447−458

■ ACKNOWLEDGMENTS

This study was supported by a grant from the National Science Foundation (MCB1837877) and a grant from the National Institutes of Health (AI125529) to M.R.

■ REFERENCES

(1) Lawrence, J. R., Korber, D. R., Hoyle, B. D., Costerton, J. W., and Caldwell, D. E. (1991) Optical sectioning of microbial biofilms. *J. Bacteriol. 173*, 6558−67.
(2) Sutherland, I. (2001) Biofilm exopolysaccharides: a strong and sticky framework. *Microbiology 147*, 3−9.
(3) Costerton, J. W., Stewart, P. S., and Greenberg, E. P. (1999) Bacterial Biofilms: A Common Cause of Persistent Infection. *Science 284*, 1318−1322.
(4) Donlan, R. M. (2001) Biofilms and device-associated infections. *Emerging Infect. Dis. 7*, 277−81.
(5) Drenkard, E., and Ausubel, F. M. (2002) *Pseudomonas* biofilm formation and antibiotic resistance are linked to phenotypic variation. *Nature 416*, 740.
(6) Winstanley, C., O'Brien, S., and Brockhurst, M. A. (2016) *Pseudomonas aeruginosa* Evolutionary Adaptation and Diversification in Cystic Fibrosis Chronic Lung Infections. *Trends Microbiol. 24*, 327−337.
(7) Fazli, M., Almblad, H., Rybtke, M. L., Givskov, M., Eberl, L., and Tolker-Nielsen, T. (2014) Regulation of biofilm formation in *Pseudomonas* and *Burkholderia* species. *Environ. Microbiol. 16*, 1961−81.
(8) Kang, D., and Kirienko, N. V. (2018) Interdependence between iron acquisition and biofilm formation in *Pseudomonas aeruginosa*. *J. Microbiol. 56*, 449−457.
(9) Weinberg, E. D. (2009) Iron Availability and Infection. *Biochim. Biophys. Acta, Gen. Subj. 1790*, 600−605.
(10) Hood, M. I., and Skaar, E. P. (2012) Nutritional immunity: transition metals at the pathogen-host interface. *Nat. Rev. Microbiol. 10*, 525−37.
(11) Benson, D. R., and Rivera, M. (2013) Heme Uptake and Metabolism in Bacteria. *Met. Ions Life Sci. 12*, 279−332.
(12) Eshelman, K., Yao, H., Punchi Hewage, A. N. D., Deay, J. J., Chandler, J. R., and Rivera, M. (2017) Inhibiting the BfrB:Bfd Interaction in *Pseudomonas aeruginosa* Causes Irreversible Iron Accumulation in Bacterioferritin and Iron Deficiency in the Bacterial Cell. *Metallocmics 9*, 646−659.
(13) Keyer, K., and Imlay, J. A. (1996) Superoxide Accelerates DNA-Damage by Elevating Free-Iron Levels. *Proc. Natl. Acad. Sci. U. S. A. 93*, 13635−13649.
(14) Forsberg, C. M., and Bullen, J. J. (1972) The Effect of Passage and Iron on the Virulence of *Pseudomonas aeruginosa*. *J. Clin. Pathol. 25*, 65−68.
(15) Hancock, R. E., and Speert, D. P. (2000) Antibiotic resistance in *Pseudomonas aeruginosa*: mechanisms and impact on treatment. *Drug Resist. Updates 3*, 247−255.
(16) Singh, P. K., Parsek, M. R., Greenberg, E. P., and Welsh, M. J. (2002) A Component of Innate Immunity Prevents Bacterial Biofilm Development. *Nature 417*, 552−555.
(17) Banin, E., Vasil, M. L., and Greenberg, E. P. (2005) Iron and *Pseuodomonas aeruginosa* biofilm formation. *Proc. Natl. Acad. Sci. U. S. A. 102*, 11076−11081.
(18) Banin, E., Brady, K. M., and Greenberg, E. P. (2006) Chelator-induced dispersal and killing of *Pseudomonas aeruginosa* cells in a biofilm. *Appl. Environ. Microbiol. 72*, 2064−9.
(19) Moreau-Marquis, S., O'Toole, G. A., and Stanton, B. A. (2009) Tobramycin and FDA-approved iron chelators eliminate Pseudomonas aeruginosa biofilms on cystic fibrosis cells. *Am. J. Respir. Cell Mol. Biol. 41*, 305−13.
(20) O'May, C. Y., Sanderson, K., Roddam, L. F., Kirov, S. M., and Reid, D. W. (2009) Iron-binding compounds impair Pseudomonas aeruginosa biofilm formation, especially under anaerobic conditions. *J. Med. Microbiol. 58*, 765−73.
(21) Kaneko, Y., Thoendel, M., Olakanmi, O., Britigan, B. E., and Singh, P. K. (2007) The Transition Metal Gallium Disrupts *Pseudomonas aeruginosa* Iron Metabolism and has Antimicrobial and Antibiofilm Activity. *J. Clin. Invest. 117*, 877−887.
(22) Banin, E., Lozinski, A., Brady, K. M., Berenshtein, E., Butterfield, P. W., Moshe, M., Chevion, M., Greenberg, E. P., and Banin, E. (2008) The potential of desferrioxamine-gallium as an anti-Pseudomonas therapeutic agent. *Proc. Natl. Acad. Sci. U. S. A. 105*, 16761−6.
(23) Goss, C. H., Kaneko, Y., Khuu, L., Anderson, G. D., Ravishankar, S., Aitken, M. L., Lechtzin, N., Zhou, G., Czyz, D. M., McLean, K., et al. (2018) Gallium disrupts bacterial iron metabolism and has therapeutic effects in mice and humans with lung infections. *Sci. Transl. Med. 10*, No. eaat7520.
(24) Punchi Hewage, A. N. D., Yao, H., Nammalwar, B., Gnanasekaran, K. K., Lovell, S., Bunce, R. A., Eshelman, K., Phaniraj, S. M., Lee, M. M., Peterson, B. R., Battaile, K. P., Reitz, A. B., and Rivera, M. (2019) Small Molecule Inhibitors of the BfrB-Bfd Interaction Decrease *Pseudomonas aeruginosa* Fitness and Potentiate Fluoroquinolone Activity. *J. Am. Chem. Soc. 141*, 8171−8184.
(25) Weeratunga, S., Lovell, S., Yao, H., Battaile, K. P., Fischer, C. J., Gee, C. E., and Rivera, M. (2010) Structural Studies of Bacterioferritin B (BfrB) from *Pseudomonas aeruginosa* Suggest a Gating Mechanism for Iron Uptake via the Ferroxidase Center. *Biochemistry 49*, 1160−1175.
(26) Rivera, M. (2017) Bacterioferritin: Structure, Dynamics and Protein-Protein Interactions at Play in Iron Storage and Mobilization. *Acc. Chem. Res. 50*, 331−340.
(27) Weeratunga, S., Gee, C. E., Lovell, S., Zeng, Y., Woodin, C. L., and Rivera, M. (2009) Binding of *Pseudomonas aeruginosa* Apobacterioferritin-Associated Ferredoxin to Bacterioferritin B Promotes Heme Mediation of Electron Delivery and Mobilization of Core Mineral Iron. *Biochemistry 48*, 7420−7431.
(28) Yao, H., Wang, Y., Lovell, S., Kumar, R., Ruvinsky, A. M., Battaile, K. P., Vakser, I. A., and Rivera, M. (2012) The Structure of the BfrB-Bfd Complex Reveals Protein-Protein Interactions Enabling Iron Release from Bacterioferritin. *J. Am. Chem. Soc. 134*, 13470−81.
(29) Wijerathne, H., Yao, H., Wang, Y., Lovell, S., Battaile, K. P., and Rivera, M. (2018) Bfd, a New Class of [2Fe-2S] Protein That Functions in Bacterial Iron Homeostasis, Requires a Structural Anion Binding Site. *Biochemistry 57*, 5533−5543.
(30) Wang, Y., Yao, H., Cheng, Y., Lovell, S., Battaile, K. P., Middaugh, C. R., and Rivera, M. (2015) Characterization of the Bacterioferritin/Bacterioferritin Associated Ferredoxin Potein-Protein Interactions in Solution and Determination of Binding Energy Hot Spots. *Biochemistry 54*, 6162−6175.
(31) Yamamoto, K., Arai, H., Ishii, M., and Igarashi, Y. (2011) Trade-off between oxygen and iron acquisition in bacterial cells at the air-liquid interface. *FEMS Microbiol. Ecol. 77*, 83−94.
(32) Friedman, L., and Kolter, R. (2004) Genes involved in matrix formation in *Pseudomonas aeruginosa* PA14 biofilms. *Mol. Microbiol. 51*, 675−90.
(33) Flemming, H. C., and Wingender, J. (2010) The biofilm matrix. *Nat. Rev. Microbiol. 8*, 623−33.
(34) Kakhlon, O., and Cabantchik, Z. I. (2002) The labile iron pool: characterization, measurement, and participation in cellular processes(1). *Free Radical Biol. Med. 33*, 1037−46.
(35) Woodmansee, A. N., and Imlay, J. A. (2002) Quantitation of intracellular free iron by electron paramagnetic resonance spectroscopy. *Methods Enzymol. 349*, 3−9.
(36) Patriquin, G. M., Banin, E., Gilmour, C., Tuchman, R., Greenberg, E. P., and Poole, K. (2008) Influence of quorum sensing and iron on twitching motility and biofilm formation in *Pseudomonas aeruginosa*. *J. Bacteriol. 190*, 662−71.
(37) Prince, R. W., Cox, C. D., and Vasil, M. L. (1993) Coordinate regulation of siderophore and exotoxin A production: molecular cloning and sequencing of the *Pseudomonas aeruginosa fur* gene. *J. Bacteriol. 175*, 2589−98.

https://dx.doi.org/10.1021/acsinfecdis.9b00398
ACS Infect. Dis. 2020, 6, 447−458

(38) Griggs, D. W., and Konisky, J. (1989) Mechanism for iron-regulated transcription of the *Escherichia coli cir* gene: metal-dependent binding of fur protein to the promoters. *J. Bacteriol. 171*, 1048−54.
(39) Ochsner, U. A., Wilderman, P. J., Vasil, A. I., and Vasil, M. L. (2002) GeneChip Expression Analysis of the Iron Starvation Response in *Pseudomonas aeruginosa*: Identification of Novel Pyoverdine Biosynthesis Genes. *Mol. Microbiol. 45*, 1277−1287.
(40) Yang, L., Barken, K. B., Skindersoe, M. E., Christensen, A. B., Givskov, M., and Tolker-Nielsen, T. (2007) Effects of iron on DNA release and biofilm development by *Pseudomonas aeruginosa*. *Microbiology 153*, 1318−28.
(41) Oglesby, A. G., Farrow, J. M., Lee, J.-H., Tomaras, A. P., Greenbergh, E. P., and Pasci, E. (2008) The Influence of Iron on *Pseudomonas aeruginosa* Physiology A regulatory Link Between Iron and Quorum sensing. *J. Biol. Chem. 283*, 15558−15567.
(42) Reinhart, A. A., Powell, D. A., Nguyen, A. T., O'Neill, M., Djapgne, L., Wilks, A., Ernst, R. K., and Oglesby-Sherrouse, A. G. (2015) The *prrF*-encoded small regulatory RNAs are required for iron homeostasis and virulence of *Pseudomonas aeruginosa*. *Infect. Immun. 83*, 863−75.
(43) Reinhart, A. A., Nguyen, A. T., Brewer, L. K., Bevere, J., Jones, J. W., Kane, M. A., Damron, F. H., Barbier, M., and Oglesby-Sherrouse, A. G. (2017) The *Pseudomonas aeruginosa* PrrF Small RNAs Regulate Iron Homeostasis during Acute Murine Lung Infection. *Infect. Immun. 85*, e00764−16.
(44) Farrow, J. M., 3rd, and Pesci, E. C. (2007) Two distinct pathways supply anthranilate as a precursor of the *Pseudomonas* quinolone signal. *J. Bacteriol. 189*, 3425−33.
(45) Berlutti, F., Morea, C., Battistoni, A., Sarli, S., Cipriani, P., Superti, F., Ammendolia, M. G., and Valenti, P. (2005) Iron Availability Influences Aggregation, Biofilm, Adhesion and Invasion of *Pseudomonas aeruginosa* and *Burkholderia cenocepacia*. *Int. J. Immunopathol. Pharmacol. 18*, 661−670.
(46) Davey, M. E., Caiazza, N. C., and O'Toole, G. A. (2003) Rhamnolipid surfactant production affects biofilm architecture in *Pseudomonas aeruginosa* PAO1. *J. Bacteriol. 185*, 1027−36.
(47) Glick, R., Gilmour, C., Tremblay, J., Satanower, S., Avidan, O., Deziel, E., Greenberg, E. P., Poole, K., and Banin, E. (2010) Increase in rhamnolipid synthesis under iron-limiting conditions influences surface motility and biofilm formation in *Pseudomonas aeruginosa*. *J. Bacteriol. 192*, 2973−80.
(48) Lequette, Y., and Greenberg, E. P. (2005) Timing and localization of rhamnolipid synthesis gene expression in *Pseudomonas aeruginosa* biofilms. *J. Bacteriol. 187*, 37−44.
(49) Caiazza, N. C., Shanks, R. M., and O'Toole, G. A. (2005) Rhamnolipids modulate swarming motility patterns of *Pseudomonas aeruginosa*. *J. Bacteriol. 187*, 7351−61.
(50) Deziel, E., Lepine, F., Milot, S., and Villemur, R. (2003) *rhlA* is required for the production of a novel biosurfactant promoting swarming motility in *Pseudomonas aeruginosa*: 3-(3-hydroxyalkanoyloxy)alkanoic acids (HAAs), the precursors of rhamnolipids. *Microbiology 149*, 2005−13.
(51) Tremblay, J., Richardson, A. P., Lepine, F., and Deziel, E. (2007) Self-produced extracellular stimuli modulate the *Pseudomonas aeruginosa* swarming motility behaviour. *Environ. Microbiol. 9*, 2622−30.
(52) Boles, B. R., Thoendel, M., and Singh, P. K. (2005) Rhamnolipids mediate detachment of *Pseudomonas aeruginosa* from biofilms. *Mol. Microbiol. 57*, 1210−23.
(53) Ochsner, U. A., Fiechter, A., and Reiser, J. (1994) Isolation, characterization, and expression in *Escherichia coli* of the *Pseudomonas aeruginosa rhlAB* genes encoding a rhamnosyltransferase involved in rhamnolipid biosurfactant synthesis. *J. Biol. Chem. 269*, 19787−95.
(54) Rahim, R., Ochsner, U. A., Olvera, C., Graninger, M., Messner, P., Lam, J. S., and Soberon-Chavez, G. (2001) Cloning and functional characterization of the *Pseudomonas aeruginosa rhlC* gene that encodes rhamnosyltransferase 2, an enzyme responsible for di-rhamnolipid biosynthesis. *Mol. Microbiol. 40*, 708−18.
(55) Bredenbruch, F., Nimtz, M., Wray, V., Morr, M., Muller, R., and Haussler, S. (2005) Biosynthetic pathway of *Pseudomonas aeruginosa* 4-hydroxy-2-alkylquinolines. *J. Bacteriol. 187*, 3630−5.
(56) Calfee, M. W., Shelton, J. G., McCubrey, J. A., and Pesci, E. C. (2005) Solubility and bioactivity of the *Pseudomonas* quinolone signal are increased by a *Pseudomonas aeruginosa*-produced surfactant. *Infect. Immun. 73*, 878−82.
(57) Stover, C. K., Pham, X. Q., Erwin, A. L., Mizoguchi, S. D., Warrener, P., Hickey, M. J., Brinkman, F. S. L., Hufnagle, W. O., Kowalik, D. J., Lagrou, M., Garber, R. L., Goltry, L., Tolentino, E., Westbrock-Wadman, S., Yuan, Y., Brody, L. L., Coulter, S. N., Folger, K. R., Kas, A., Larbig, K., Lim, R., Simith, K., Spencer, D., Wong, G. K. S., Wu, Z., Paulsen, I. T., Reizer, J., Saler, M. H., Hancock, R. E. W., Lory, S., and Olson, M. V. (2000) Complete Genome Sequence of *Pseudomonas aeruginosa* PA01, an Opportunistic Pathogen. *Nature 406*, 959−964.
(58) Choi, K. H., and Schweizer, H. P. (2006) mini-Tn7 insertion in bacteria with single *att*Tn7 sites: example *Pseudomonas aeruginosa*. *Nat. Protoc. 1*, 153−61.
(59) Choi, K. H., Mima, T., Casart, Y., Rholl, D., Kumar, A., Beacham, I. R., and Schweizer, H. P. (2008) Genetic tools for select-agent-compliant manipulation of *Burkholderia pseudomallei*. *Appl. Environ. Microbiol. 74*, 1064−75.
(60) Clark, J., and Maaløe, O. (1967) DNA Replication and the Division Cycle in *Escherichia coli*. *J. Mol. Biol. 23*, 99−112.
(61) Merritt, J. H., Kadouri, D. E., and O'Toole, G. A. (2005) Growing and analyzing static biofilms. *Curr Protoc Microbiol* Chapter 1. *Unit 1B*, 1.
(62) Heydorn, A., Nielsen, A. T., Hentzer, M., Sternberg, C., Givskov, M., Ersboll, B. K., and Molin, S. (2000) Quantification of biofilm structures by the novel computer program COMSTAT. *Microbiology 146*, 2395−407.
(63) Otsu, N. (1979) A Threshold Selection Method for Gray-Level Histograms. *IEEE Transactions on Systems, Man, and Cybernetics 9*, 62−66.
(64) Meyer, J. M., and Abdallah, M. A. (1978) The Fluorescent Pigment of *Pseudomonas fluorescens*: Biosynthesis, Purification and Physicochemical Properties. *J. Gen. Microbiol. 107*, 319−328.
(65) Fish, W. W. (1988) Rapid colorimetric micromethod for the quantitation of complexed iron in biological samples. *Methods Enzymol. 158*, 357−64.
(66) Berlett, B. S., Levine, R. L., Chock, P. B., Chevion, M., and Stadtman, E. R. (2001) Antioxidant activity of Ferrozine-iron-amino acid complexes. *Proc. Natl. Acad. Sci. U. S. A. 98*, 451−6.
(67) Riemer, J., Hoepken, H. H., Czerwinska, H., Robinson, S. R., and Dringen, R. (2004) Colorimetric ferrozine-based assay for the quantitation of iron in cultured cells. *Anal. Biochem. 331*, 370−5.
(68) Lepine, F., Milot, S., Deziel, E., He, J., and Rahme, L. G. (2004) Electrospray/mass spectrometric identification and analysis of 4-hydroxy-2-alkylquinolines (HAQs) produced by *Pseudomonas aeruginosa*. *J. Am. Soc. Mass Spectrom. 15*, 862−9.
(69) Pinzon, N. M., and Ju, L. K. (2009) Analysis of rhamnolipid biosurfactants by methylene blue complexation. *Appl. Microbiol. Biotechnol. 82*, 975−81.
(70) Wittgens, A., Tiso, T., Arndt, T. T., Wenk, P., Hemmerich, J., Muller, C., Wichmann, R., Kupper, B., Zwick, M., Wilhelm, S., Hausmann, R., Syldatk, C., Rosenau, F., and Blank, L. M. (2011) Growth independent rhamnolipid production from glucose using the non-pathogenic *Pseudomonas putida* KT2440. *Microb. Cell Fact. 10*, 80.
(71) Inoue, T., Shingaki, R., and Fukui, K. (2008) Inhibition of swarming motility of *Pseudomonas aeruginosa* by branched-chain fatty acids. *FEMS Microbiol. Lett. 281*, 81−6.

https://dx.doi.org/10.1021/acsinfecdis.9b00398
ACS Infect. Dis. 2020, 6, 447−458